

# Exact results relating spin-orbit interactions in two dimensional strongly correlated systems

Nóra Kucska and Zsolt Gulácsi

*Department of Theoretical Physics, University of Debrecen,  
H-4010 Debrecen, Bem ter 18/B, Hungary*

(Dated: February 18, 2022)

## Abstract

A 2D square, two-bands, strongly correlated and non-integrable system is analysed exactly in the presence of many-body spin-orbit interactions via the method of Positive Semidefinite Operators. The deduced exact ground states in the high concentration limit are strongly entangled, and given by the spin-orbit coupling are ferromagnetic and present an enhanced carrier mobility, which substantially differs for different spin projections. The described state emerges in a restricted parameter space region, which however is clearly accessible experimentally. The exact solutions are provided via the solution of a matching system of equations containing 74 coupled, non-linear and complex algebraic equations. In our knowledge, other exact results for 2D interacting systems with spin-orbit interactions are not present in the literature.

PACS numbers: PACS No. 71.10.Fd, 71.10.Hf, 71.10 Pm, 71.70.Ej, 05.30.Fk, 67.40.Db

## I. INTRODUCTION

The many-body spin-orbit interaction (SOI) plays an essential role in the physics of surfaces and interfaces in a continuously increasing number of systems of large interest. Indeed, large SOI coupling is present at interfaces between heavy elements (e.g. Pb, Sb, Bi) and non-magnetic materials as Ag, Au, Cu, which can lead to surface density waves<sup>1</sup>, manipulation possibility of spin-orbit splitting by surface alloying<sup>2</sup>, or charge- to spin-current conversion<sup>3</sup> with application possibility in spintronics; semiconductor reconstructed surfaces using heavy elements as in the case of Pb on Ge(1,1,1)<sup>4</sup>, Bi or Tl on Si(1,1,1)<sup>5</sup>, or Au on Ge(1,1,1)<sup>6</sup> which can lead to spin control in electronic transport applications<sup>7</sup>; metal-quantum dot configurations influencing transport properties of Aharonov-Bohm rings<sup>8</sup>; graphene layers on metallic substrates<sup>9</sup> influencing the transport properties of graphene<sup>10</sup>, leads to band splitting and enriched spintronic effects<sup>11</sup> and influences topological insulator properties<sup>12</sup>; complex oxide interfaces as for example in the case of  $LaAlO_3/SrTiO_3$ <sup>13,14</sup> which even can provide tunable superconductivity at the interface<sup>15</sup>; or pnictogen 2D honeycomb type of lattices presenting as well magnetic properties<sup>16</sup>. Also in other cases the SOI interaction plays an important role in the magnetic behaviour of surfaces and interfaces<sup>17</sup>. Indeed, magnetism can appear at the interface of two, otherwise non-magnetic perovskites<sup>18</sup>; at the interface between  $Cr_2O_3$  and overlayers of Pd or Pt<sup>19</sup>; Cu or Mn in thin films interfaced with organic molecules<sup>20</sup>; nanoparticle surfaces with extremely high surface/volume ratio fabricated from otherwise macroscopically non-magnetic materials (e.g. Au, or Pd)<sup>21,22</sup>; or interfaces in multilayers<sup>23</sup>. In several of these cases also anomalous magneto-transport measurements have been reported<sup>8,17,24</sup>.

When SOI is effective at the interface, often it happens that also the inter electronic interaction is strong, i.e. the system is strongly correlated. This is the case of metal - quantum dot - metal configurations<sup>8</sup>; interfaces present in between complex oxides or perovskites<sup>18</sup>; osmate double perovskites<sup>25</sup>; GaAs heterostructures<sup>24</sup>; iridates<sup>26</sup>, iridium based heterostructures<sup>27</sup> or iridates in perovskite- and honeycomb-based structures<sup>28</sup>; and even heterostructures with organic materials<sup>20</sup>. In these strongly correlated systems, the effect of the spin-orbit interaction is not yet well understood<sup>26</sup>, the band splitting (caused by SOI) in the presence of the inter electronic interaction even considered a fundamental effect is not understood in details<sup>24</sup>, the interplay of strong electron correlation and large SOI is relatively less explored<sup>25</sup>, and

perturbative treatment being inconclusive cannot be applied<sup>28</sup>. From the other side is known that SOI has major effects on basic model results describing strong correlations as in the case of the Hubbard model<sup>29</sup>, periodic Anderson model<sup>30</sup>, or Bethe ansatz exact solutions derived for integrable cases, which are strongly affected<sup>31</sup>. Furthermore, often correlations even enhance SOI<sup>32</sup>, or vice versa, SOI provides mechanism for strong correlation effects as e.g. in the case of metal-insulator transition<sup>34</sup>, and that multi-orbital treatment is important for the description of effects caused by SOI<sup>32,33</sup>. Till today such systems have been analysed only by exact diagonalization technique on small samples<sup>32</sup>, non-equilibrium Green-function techniques<sup>8</sup>, and finally, numerical procedures e.g. variational Monte Carlo<sup>35</sup>, Monte Carlo simulations combined with spin-wave theory<sup>36</sup>, or density-functional theory based approximations<sup>33</sup>.

Contrary to the importance of this field, exact results relating 2D strongly correlated systems containing SOI are not known today. The difficulty of this job lies in the fact that such systems are non-integrable, and because of this reason, only special techniques are possible to be applied in order to deduce exact results. In this paper we begin to fill up this gap by presenting in our knowledge the first 2D exact ground states for a two band strongly correlated system containing SOI, using the method of positive semidefinite operators whose applicability does not depend on dimensionality and integrability<sup>37–39</sup>, (see also the review in Ref.[<sup>40</sup>]). One notes, that the method has been previously applied in conditions unimaginable before in the context of exact solutions, as disordered systems in 2D [<sup>41</sup>]; multiband systems in 2D [<sup>42</sup>] and 3D [<sup>43</sup>]; stripe, checkerboard and droplet states in 2D [<sup>44</sup>]; delocalization effect of the Hubbard repulsion in 2D [<sup>45</sup>]; or different non-integrable chain structures<sup>38,39,46–48</sup>. Here we focus on magnetic properties and show that given by the interplay of SOI and correlations, ferromagnetism is possible to be induced on surfaces and interfaces increasing in the same time, differentiated for different spin projections, the mobility of carriers.

The remaining part of the paper is structured as follows: Section II. describes the studied system, Section III. presents an insight in the physical behavior of the system, Section IV. shows the transformation in positive semidefinite form of the Hamiltonian, Section V. deduces the exact ground states, Section VI. analyses the physical properties of the deduced ground states, and finally, the Summary and Conclusions in Section VII. closes the presentation. The three Appendices A,B,C contain the mathematical details of the deductions.

## II. THE SYSTEM ANALYSED

One analyses a square itinerant system in two dimensions ( $2D$ ) containing a correlated band (denoted hereafter by  $f$ ) which experiences the action of the on-site Coulomb repulsion  $U_f > 0$ , and is hybridised with a non-correlated band (denoted for simplicity by  $d$ ). The one particle part ( $\hat{H}_{kin}$ ) of the Hamiltonian ( $\hat{H}$ ) contains besides on-site one-particle potentials ( $\epsilon$ ), on-site ( $V_0$ ) and nearest-neighbor ( $V_{i,j}$ ) hybridizations, also nearest-neighbor hopping terms ( $t_{i,j}^f, t_{i,j}^d$ ). In between the hopping terms, given by the many-body spin-orbit interactions, also spin-flip hopping terms are present. In these conditions, using the notations  $c = d, f$ , and  $\mathbf{p} = \mathbf{x}, \mathbf{y}$ , where  $\mathbf{x}$  and  $\mathbf{y}$  are representing the Bravais vectors of the  $2D$  system, introducing the local

$$\hat{H}_{c,0} = \sum_{\mathbf{i}} \sum_{\alpha=\uparrow,\downarrow} \epsilon_c^{\alpha,\alpha} \hat{c}_{\mathbf{i},\alpha}^\dagger \hat{c}_{\mathbf{i},\alpha}, \quad \hat{V}_0 = \sum_{\mathbf{i}} [(\sum_{\alpha=\uparrow,\downarrow} V_0^{d,f,\alpha,\alpha} \hat{d}_{\mathbf{i},\alpha}^\dagger \hat{f}_{\mathbf{i},\alpha}) + H.c.], \quad (1)$$

and nearest-neighbor

$$\begin{aligned} \hat{H}_{c,\mathbf{p}} &= \sum_{\mathbf{i}} [(\sum_{\alpha=\uparrow,\downarrow} t_{\mathbf{p}}^{c,\uparrow,\uparrow} \hat{c}_{\mathbf{i}+\mathbf{p},\alpha}^\dagger \hat{c}_{\mathbf{i},\alpha}) + t_{\mathbf{p}}^{c,\downarrow,\uparrow} \hat{c}_{\mathbf{i}+\mathbf{p},\downarrow}^\dagger \hat{c}_{\mathbf{i},\uparrow} + t_{\mathbf{p}}^{c,\uparrow,\downarrow} \hat{c}_{\mathbf{i}+\mathbf{p},\uparrow}^\dagger \hat{c}_{\mathbf{i},\downarrow} + H.c.], \\ \hat{V}_{\mathbf{p}} &= \sum_{\mathbf{i}} [\sum_{\alpha=\uparrow,\downarrow} (V_{\mathbf{p}}^{d,f,\alpha,\alpha} \hat{d}_{\mathbf{i}+\mathbf{p},\alpha}^\dagger \hat{f}_{\mathbf{i},\alpha} + V_{\mathbf{p}}^{f,d,\alpha,\alpha} \hat{f}_{\mathbf{i}+\mathbf{p},\alpha}^\dagger \hat{d}_{\mathbf{i},\alpha}) + H.c.], \end{aligned} \quad (2)$$

one-particle contributions, one obtains for  $\hat{H} = \hat{H}_{kin} + \hat{H}_{int}$  the expressions

$$\begin{aligned} \hat{H}_{kin} &= \hat{V}_0 + \sum_{\mathbf{p}=\mathbf{x},\mathbf{y}} [\hat{V}_{\mathbf{p}} + \sum_{c=d,f} (\hat{H}_{c,0} + \hat{H}_{c,\mathbf{p}})], \\ \hat{H}_{int} &= \sum_{\mathbf{i}} U_f \hat{n}_{\mathbf{i},\uparrow}^f \hat{n}_{\mathbf{i},\downarrow}^f, \end{aligned} \quad (3)$$

where  $\hat{c}_{\mathbf{j},\alpha}$ , for  $c = d, f$  are canonical Fermi operators, and  $\hat{n}_{\mathbf{i},\alpha}^f = \hat{f}_{\mathbf{i},\alpha}^\dagger \hat{f}_{\mathbf{i},\alpha}$ . As seen from the last row of Eq.(3), the inter-electronic interaction term is represented by the Hubbard interaction in the correlated band. As was mentioned above, the spin-flip hopping contributions in  $\hat{H}_{c,\mathbf{p}}$  originate from the many-body spin-orbit interactions. Often, these interactions are taken into account on a phenomenological ground<sup>29,49,50</sup>. But one notes that usually such terms emerge via the Rashba and Dresselhaus contributions which for 2D square lattice provide

$$\hat{H}_{SO,c} = \sum_{\mathbf{i}} [\sum_{\mathbf{p}=\mathbf{x},\mathbf{y}} (V_{\uparrow,\downarrow}^{c,\mathbf{p}} \hat{c}_{\mathbf{i}+\mathbf{p},\uparrow}^\dagger \hat{c}_{\mathbf{i},\downarrow} + V_{\downarrow,\uparrow}^{c,\mathbf{p}} \hat{c}_{\mathbf{i}+\mathbf{p},\downarrow}^\dagger \hat{c}_{\mathbf{i},\uparrow}) + H.c.], \quad (4)$$

where, for fixed  $c$ , one has  $V_{\uparrow,\downarrow}^{c,\mathbf{x}} = V_R^c - iV_D^c$ ,  $V_{\downarrow,\uparrow}^{c,\mathbf{x}} = -V_R^c - iV_D^c$ ,  $V_{\uparrow,\downarrow}^{c,\mathbf{y}} = V_D^c - iV_R^c$ ,  $V_{\downarrow,\uparrow}^{c,\mathbf{y}} = -V_D^c - iV_R^c$ , the notation  $V_R^c$ ,  $V_D^c$  signaling the Rashba, and Dresselhaus interaction strengths respectively, see [51]. With the contributions presented in Eq.(4), one has e.g.  $t_{\mathbf{p}}^{c,\uparrow,\downarrow} = V_{\uparrow,\downarrow}^{c,\mathbf{p}}$ , etc.

As we mentioned in the Introduction, the SOI effects in the presence of strong correlations must be treated at multibands level. Exactly for this reason, we present our study for a two-band type of structure. On this line we note that the presence of two bands does not diminish the applicability of the deduced results because for a multiband material the theoretical description is given usually by projecting the multiband structure in a few-band picture<sup>52</sup>, which is stopped here only for its relative simplicity at two-bands level.

### III. INSIGHT IN THE PHYSICAL BEHAVIOR OF THE SYSTEM

In order to present an insight in the physical behavior of the system let us concentrate on the bare band structure (see Appendix B) provided by  $\hat{H}_{kin}$ . For simplicity we exemplify by using  $\mathbf{k}_y = 0$  plots, the first Brillouin zone in  $\mathbf{k}_x$  direction being placed in between the dashed lines (note that all directions present similar qualitative behavior). Fig.1a shows a pedagogical band structure without spin-flip terms i.e. without spin-orbit interactions. As it can be observed, each energy band is double degenerated containing both spin projections. Fig.1b exemplifies what is happening when spin-flip contributions are turned on: the double spin-projection degeneracy is lifted. The resulting  $\pm$  bands are no more spin-projection degenerated. This notation underlines that now the resulting non-degenerate bands contain usually all spin projections but with different weights.

Following the pedagogical example from Fig.1, the plot presented in Fig.2 shows a band structure emerging together with the spin-orbit contributions present in the Hamiltonian, containing the input from (4) and leading to  $\epsilon_{d,\mathbf{k}}^{\uparrow,\downarrow} = 2t_x^{d,\uparrow,\downarrow}(i \sin \mathbf{k}\mathbf{x} + e^{i\chi} \cos \mathbf{k}\mathbf{y})$ ,  $\epsilon_{f,\mathbf{k}}^{\uparrow,\downarrow} = 2t_x^{f,\uparrow,\downarrow}(i \sin \mathbf{k}\mathbf{x} + e^{i\chi} \cos \mathbf{k}\mathbf{y})$  defined for the band structure calculation in Appendix B. As seen in Fig.2, the spin projection degeneracy, as before is lifted, the motivation for the  $\pm$  notation is as explained for Fig.1.

This lifted spin projection degeneracy produces the peculiarities measured on surfaces in the presence of the spin-orbit interactions which are seen as well e.g. in magnetotransport<sup>3,18</sup>, or magnetic behavior<sup>17,20,23,53</sup>.

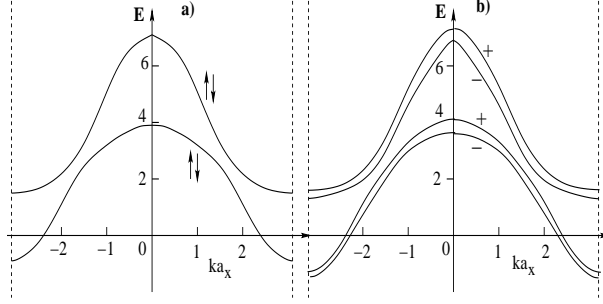


FIG. 1: a) The band structure without spin-flip contributions. All parameters are expressed in  $t_x^{d,\sigma,\sigma} = t_x^d$  units and not depend on the  $\sigma$  value (i.e. the parameter values for  $\uparrow, \uparrow$ , and  $\downarrow, \downarrow$  indices are equal). In the provided example, non-zero parameters are  $t_x^{d,\uparrow,\uparrow} = 1.0$ ;  $t_y^{d,\uparrow,\uparrow} = 1.1$ ;  $\epsilon_d^{\uparrow,\uparrow} = 0.5$ ;  $t_x^{f,\uparrow,\uparrow} = 1.5$ ;  $t_y^{f,\uparrow,\uparrow} = 1.6$ ;  $\epsilon_f^{\uparrow,\uparrow} = 0.1$ ;  $V_0^{d,f,\uparrow,\uparrow} = -1.2$ ;  $V_x^{d,f,\uparrow,\uparrow} = V_x^{f,d,\uparrow,\uparrow} = 0.6$ ;  $V_y^{d,f,\uparrow,\uparrow} = V_y^{f,d,\uparrow,\uparrow} = 0.7$ . b) Spin-flip terms are turned on. In this example, besides the a) non-zero parameters, one also has  $\epsilon_d^{\uparrow,\downarrow} = 0.2$ ;  $\epsilon_f^{\uparrow,\downarrow} = 0.25$ . For the  $\pm$  band notation see text.

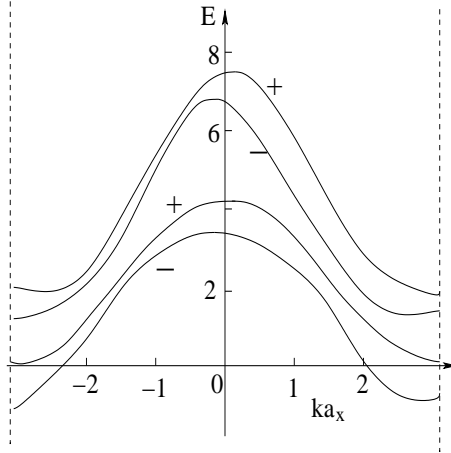


FIG. 2: Band structure in the presence of spin-orbit interaction considered in the present paper, see text. The nonzero  $\hat{H}_{kin}$  parameters are as in Fig.1a, besides which also  $t_x^{d,\uparrow,\downarrow} = 0.1$ ,  $t_x^{f,\uparrow,\downarrow} = 0.25$ ,  $\chi = \pi/2$  are considered. The energy and all  $\hat{H}_{kin}$  parameters are expressed in  $t_x^d$  units. Note that  $\mathbf{k} \cdot \mathbf{a}_y \neq 0$  holds.

The presented observations motivated our efforts to analyze in exact terms the effects of spin-orbit interactions on surfaces: can or not such contribution, in the presence of inter-electronic interactions produce surface ferromagnetism in multiband systems which are often strongly correlated? The exact study is necessary because i) spin-orbit contributions are usually relatively small in comparison to other system parameters emerging in strongly

correlated systems, and ii) as presented in the introduction, low or moderate order approximations do not provide reliable information in this field. The results of our study are presented below providing a positive answer to the above formulated question.

#### IV. THE HAMILTONIAN TRANSFORMED IN POSITIVE SEMIDEFINITE FORM

Since the analysed system is strongly correlated and our aim is to provide essential non-altered information for it, we deduce exact results in our study. Taking into account that the model used for description is a 2D non-integrable model, special techniques must be used for this purpose. Because of this reason, as we mentioned previously, one uses below a technique based on positive semidefinite operator properties.

The first step of the technique transforms in exact terms the system Hamiltonian in a positive semidefinite form

$$\hat{H} = \hat{P} + C \quad (5)$$

where  $\hat{P}$  is a positive semidefinite operator and  $C$  is a scalar. In the present case, since  $\hat{H}$  in (3) contains spin-flip terms as well, one uses for this transformation for the first time block operators that mix the spin indices. For each unit cell defined at the lattice site  $\mathbf{i}$ , one introduces two block operators  $\hat{A}_{\mathbf{i}}$  and  $\hat{B}_{\mathbf{i}}$ , denoted for simplicity by  $G = A, B$ , where one has

$$\hat{G}_{\mathbf{i}} = \sum_{c=d,f} \sum_{\alpha=\uparrow,\downarrow} (g_{G,c,1,\alpha} \hat{c}_{\mathbf{i},\alpha} + g_{G,c,2,\alpha} \hat{c}_{\mathbf{i}+\mathbf{x},\alpha} + g_{G,c,3,\alpha} \hat{c}_{\mathbf{i}+\mathbf{x}+\mathbf{y},\alpha} + g_{G,c,4,\alpha} \hat{c}_{\mathbf{i}+\mathbf{y},\alpha}), \quad (6)$$

where  $g_{G,c,n,\alpha}$  for each fixed  $G$  represent 16 numerical prefactors (i.e.  $c = d, f$ ,  $\alpha = \uparrow, \downarrow$ ,  $n = 1, 2, 3, 4$ ) which, given by the Bravais translational symmetry of the system, are the same in each cell defined at arbitrary site  $\mathbf{i}$ . In fact the block operators  $\hat{G}_{\mathbf{i}}$  are linear combinations of fermionic annihilation operators  $\hat{c}_{\mathbf{j},\alpha}$ , for all  $c = d, f$  and  $\alpha = \uparrow, \downarrow$ , acting on the four sites of the unit cell defined at the lattice site  $\mathbf{i}$  containing the four sites  $\mathbf{i}, \mathbf{i} + \mathbf{x}, \mathbf{i} + \mathbf{x} + \mathbf{y}, \mathbf{i} + \mathbf{y}$ , numbered (anti clockwise starting from  $\mathbf{i}$ ) by the in-cell site index  $n = 1, 2, 3, 4$  (see Fig.1).

Using the introduced block operators, the Hamiltonian transformed in positive semidefinite form (5) becomes

$$\hat{P} = \hat{P}_G + \hat{P}_1, \quad \hat{P}_G = \sum_{\mathbf{i}} \sum_{G=A,B} \hat{G}_{\mathbf{i}} \hat{G}_{\mathbf{i}}^\dagger, \quad \hat{P}_1 = U_f \sum_{\mathbf{i}} \hat{P}_{\mathbf{i}},$$

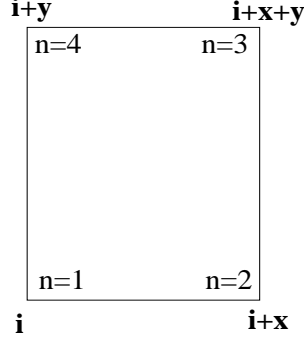


FIG. 3: Unit cell defined at the lattice site  $\mathbf{i}$  with in-cell notations of sites  $n = 1, 2, 3, 4$ . The Bravais vectors of the 2D lattice are denoted by  $\mathbf{x}$  and  $\mathbf{y}$ .

$$C = \eta N - U_f N_{sit} - \sum_{G=A,B} \sum_{\mathbf{i}} z_{\mathbf{i}}^G, \quad U_f > 0, \quad (7)$$

where  $N$  represents the number of electrons,  $N_{sit}$  gives the number of lattice sites,  $z_{\mathbf{i}}^G = \{\hat{G}_{\mathbf{i}}, \hat{G}_{\mathbf{i}}^\dagger\}$ ,  $\eta$  is a numerical parameter determined by the matching equations [see (A23)], while the positive semidefinite operator  $\hat{P}_{\mathbf{i}} = \hat{n}_{\mathbf{i},\uparrow}^f \hat{n}_{\mathbf{i},\uparrow}^f - (\hat{n}_{\mathbf{i},\uparrow}^f + \hat{n}_{\mathbf{i},\uparrow}^f) + 1$  attains its minimum eigenvalue zero when at least one electron is present on the site  $\mathbf{i}$ . One notes that in obtaining (7), periodic boundary conditions have been used in both directions.

The matching equations corresponding to the transformation (5,7) (since are representing a coupled non-linear system of 74 equations) are presented together with their solution in Appendix A. These equations provide the block operator parameters  $g_{G,c,n,\alpha}$  and the prefactor  $\eta$  [see (7)] in function of the Hamiltonian parameters present in (3) (i.e.  $t_{\mathbf{p}}^{c,\alpha,\alpha'}$ ,  $V_{\mathbf{p}}^{c,c',\alpha,\alpha'}$ ,  $\epsilon_c^{\alpha,\alpha'}$ ,  $V_0^{c,c',\alpha,\alpha'}$ ,  $U_f$ ). One needs two block operators  $G = A, B$  in order to cancel out from (7) the contributions not present in the starting  $\hat{H}$  described in (3). The matching equations are obtained by effectuating the operations presented in the right side of (7) and equating each obtained term with a given operator structure with the same operator term present in the starting Hamiltonian (3). For example, from the first row of (7), for the hopping term  $\hat{d}_{\mathbf{i}+\mathbf{x}+\mathbf{y},\uparrow}^\dagger \hat{d}_{\mathbf{i},\uparrow}$ , we obtain the coefficient  $-(g_{A,d,3,\uparrow}^* g_{A,d,1,\uparrow} + g_{B,d,3,\uparrow}^* g_{B,d,1,\uparrow})$ . But the hopping term  $\hat{d}_{\mathbf{i}+\mathbf{x}+\mathbf{y},\uparrow}^\dagger \hat{d}_{\mathbf{i},\uparrow}$ , being cell-diagonal (i.e. next nearest-neighbor hopping), is not present in the starting  $\hat{H}$  from (3). Hence the matching equation corresponding to this hopping term becomes  $g_{A,d,3,\uparrow}^* g_{A,d,1,\uparrow} + g_{B,d,3,\uparrow}^* g_{B,d,1,\uparrow} = 0$ . Similarly, for the hopping term  $\hat{d}_{\mathbf{i}+\mathbf{x},\uparrow}^\dagger \hat{d}_{\mathbf{i},\uparrow}$ , from the first row of (7) one obtains the coefficient  $-(g_{A,d,2,\uparrow}^* g_{A,d,1,\uparrow} + g_{A,d,3,\uparrow}^* g_{A,d,4,\uparrow} + g_{B,d,2,\uparrow}^* g_{B,d,1,\uparrow} + g_{B,d,3,\uparrow}^* g_{B,d,4,\uparrow})$ . In the starting Hamiltonian



(3), the  $\hat{d}_{\mathbf{i}+\mathbf{x},\uparrow}^\dagger, \hat{d}_{\mathbf{i},\uparrow}$  hopping term has the coefficient  $t_{\mathbf{x}}^{d,\uparrow,\uparrow}$ , hence the corresponding matching equation becomes  $-t_{\mathbf{x}}^{d,\uparrow,\uparrow} = g_{A,d,2,\uparrow}^* g_{A,d,1,\uparrow} + g_{A,d,3,\uparrow}^* g_{A,d,4,\uparrow} + g_{B,d,2,\uparrow}^* g_{B,d,1,\uparrow} + g_{B,d,3,\uparrow}^* g_{B,d,4,\uparrow}$ . All matching equations presented in details (together with their solution) in Appendix A, have been obtained in the same fashion.

## V. THE DEDUCED EXACT GROUND STATE WAVE FUNCTIONS

Since the lowest possible eigenvalue of a positive semidefinite operator is zero, once one has the Hamiltonian written in the positive semidefinite form (5), the exact ground state corresponding to (5) can be obtained in a second step, by constructing the most general wave vector  $|\Psi_g\rangle$  which satisfies the relation  $\hat{P}|\Psi_g\rangle = 0$ . Several techniques have been worked out for this purpose<sup>40</sup>. In the present case, the ground state wave vector, in the unnormalized form, has the expression

$$|\Psi_g\rangle = \prod_{\mathbf{i}} [(\prod_{G=A,B} \hat{G}_{\mathbf{i}}^\dagger) \hat{D}_{\mathbf{i}}^\dagger |0\rangle], \quad \hat{D}_{\mathbf{i}}^\dagger = (\gamma_\uparrow \hat{f}_{\mathbf{i},\uparrow}^\dagger + \gamma_\downarrow \hat{f}_{\mathbf{i},\downarrow}^\dagger), \quad (8)$$

where  $\gamma_\alpha$ ,  $\alpha = \uparrow, \downarrow$  are numerical prefactors,  $\prod_{\mathbf{i}}$  extends over all  $N_{sit}$  lattice sites, and  $|0\rangle$  is the bare vacuum with no fermions present. Note that (8) corresponds to  $N = 3N_{sit} = (3/4)N_{tot}$  electrons in the system, where  $N_{tot} = 4N_{sit}$  represents the electron number at complete system filling. The block operator parameters of  $\hat{G}_{\mathbf{i}}^\dagger$  operators are obtained as solutions of the matching equations and are explicitly deduced and presented in Appendix A.

The  $|\Psi_g\rangle$  wave vector represents the ground state for the following reasons: i) The  $\hat{G}_{\mathbf{i}}^\dagger$  operators are linear combinations of canonical Fermi operators acting on the sites of a finite block, hence the equality  $\hat{G}_{\mathbf{i}}^\dagger \hat{G}_{\mathbf{i}}^\dagger = 0$  holds. Consequently  $\hat{P}_G |\Psi_g\rangle = 0$  is automatically satisfied. Furthermore, ii) the  $\hat{P}_1$  operator attains its minimum eigenvalue zero when at least one f-electron is present on all lattice sites  $\mathbf{i}$ . But  $\prod_{\mathbf{i}} \hat{D}_{\mathbf{i}}^\dagger$  introduces at least one f-electron on all sites. As a consequence,  $\hat{P}_1 |\Psi_g\rangle = 0$  also holds, hence for  $\hat{P} = \hat{P}_G + \hat{P}_1$  the requirement  $\hat{P} |\Psi_g\rangle = 0$  is satisfied. We note that the uniqueness of  $|\Psi_g\rangle$  from (8) can also be demonstrated on the line of Appendix B from Ref.[<sup>40</sup>].

We underline that (8) represents a highly entangled many-body ground state. Indeed, if the products are effectuated from its expression,  $|\Psi_g\rangle$  becomes to be a huge sum over many orthogonal contributions. Furthermore, if at least one individual operator connected to an arbitrary  $\mathbf{i}$  site is missing from the  $|\Psi_g\rangle$  expression, (8) is no more the ground state of the

studied Hamiltonian. Finally, individual contributions taken from the right side of (8) are not representing one particle eigenstates, hence the strongly entangled many-body nature of  $|\Psi_g\rangle$  is clearly visible from its expression.

One notes that the ground state (8) can also be extended above  $N^* = 3N_{sit}$  to total particle number  $N = N^* + N_1$ , where  $N_1 < N_{sit}$ . Indeed one has

$$|\Psi_g(N > N^*) = \prod_{\mathbf{i}} [(\prod_{G=A,B} \hat{G}_{\mathbf{i}}^\dagger) \hat{D}_{\mathbf{i}}^\dagger] \hat{F}^\dagger |0\rangle, \quad \hat{F}^\dagger = \prod_{\delta=1}^{N_1} \hat{c}_{\delta, \mathbf{k}_\delta, \sigma_\delta}^\dagger, \quad (9)$$

where  $c_\delta$  can be arbitrarily  $d, f$ ;  $\sigma_\delta$  is an arbitrary spin projection, and  $\mathbf{k}_\delta$  is an arbitrary momentum from the first Brillouin zone. This is because for  $N > N^*$ , the conditions i) and ii) described below (8) are both satisfied, (9) remaining as well a strongly entangled ground state.

## VI. THE GROUND STATE PHYSICAL PROPERTIES

Once the exact ground state is known, the third step of the method follows, namely the deduction of the physical properties of the ground state. This is done by calculating ground state expectation values for quantities of interest. In this section we deduce in details ground state expectation values at  $N = N^*$  number of particles using the ground state (8). The calculations are done in  $\mathbf{k}$  space representation (see for details Appendix C).

### A. The total $S^z$ ground state expectation value

First, in order to test magnetization properties we calculate the total  $\hat{S}^z$  ground state expectation value, where

$$\hat{S}^z = \sum_{\mathbf{k}} \sum_{c=d,f} \hat{S}_{c,\mathbf{k}}^z, \quad \hat{S}_{c,\mathbf{k}}^z = \frac{1}{2}(\hat{n}_{\mathbf{k},\uparrow}^c - \hat{n}_{\mathbf{k},\downarrow}^c), \quad (10)$$

where the sum over  $\mathbf{k}$  runs over the first Brillouin zone. Furthermore the expectation values for an arbitrary operator  $\hat{X}$  are standardly deduced via  $\langle \hat{X} \rangle = \langle \Psi_g | \hat{X} | \Psi_g \rangle / \langle \Psi_g | \Psi_g \rangle$ . Calculation details are presented in Appendix C: the norm  $\langle \Psi_g | \Psi_g \rangle$  is present in (C4), the  $\langle \hat{S}^z \rangle / N_{sit}$  ratio, whose magnitude is denoted by  $\bar{S}^z$  in Fig.4, is given in (C6). One finds for  $\bar{S}^z$  the result presented in Fig.4. As can be seen, the ground state expectation value of the

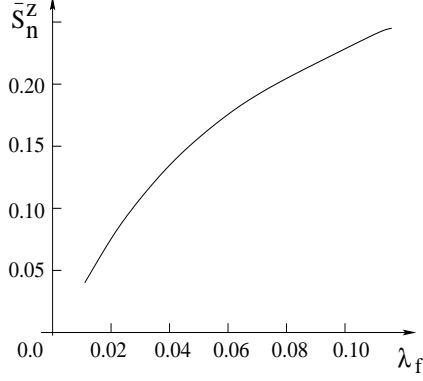


FIG. 4: The normalized total  $\hat{S}^z$  ground state expectation value  $\bar{S}_n^z = \bar{S}^z / \bar{S}_{Max}^z$  in function of the effective spin-orbit interaction  $\lambda_f = (|V_R^f|^2 + |V_D^f|^2)^{1/2}$  in the correlated f-band, where  $\lambda_f$  is given in  $t_x^{f,\sigma,\sigma}$  units. Note that  $\bar{S}_{Max}^z = 1/2$  relation holds.

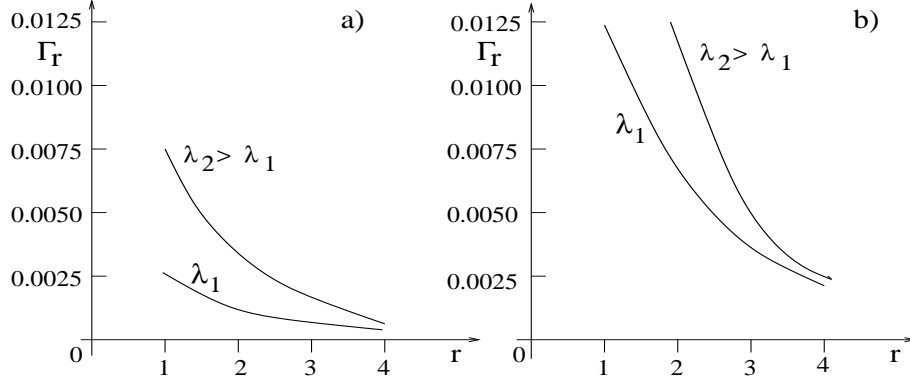


FIG. 5: The  $\mathbf{r}$  dependent hopping ground state expectation value  $\Gamma_{\mathbf{r}}$  in function of the effective total spin-orbit interaction  $\lambda = (1/2) \sum_{c=d,f} \lambda_c$  exemplified for d electrons in  $\mathbf{x}$  direction. The distance  $\mathbf{r}$  is given in lattice constant units. In the plot one has in  $t_x^{f,\sigma,\sigma}$  units  $\lambda_1 = 0.0185$ , and  $\lambda_2 = 0.0495$ , respectively. Note that if  $\lambda$  increases,  $\Gamma_{\mathbf{r}}$  increases as well and one has a strong spin projection dependence. The presented cases: a) negative spin projection to the Z axis, and b) positive spin projection to the Z axis.

total  $\hat{S}^z$  spin increases with the effective spin-orbit interaction  $\lambda_c = (|V_R^c|^2 + |V_D^c|^2)^{1/2}$  in the correlated i.e. c=f band. The normalized value  $\bar{S}_n^z$  continuously decreases with  $\lambda_f$  within the parameter space region in which (8) is valid, signaling that  $\langle \hat{S}^z \rangle$  is non-zero given by the effective spin-orbit interaction in the correlated band<sup>54</sup>. Furthermore since  $\langle \hat{S}^z \rangle \neq 0$  automatically implies  $\langle \hat{S}^2 \rangle \neq 0$  where  $\hat{S}^2$  is the square of the total spin, it results that the deduced ground state is ferromagnetic.

## B. The $\mathbf{r}$ dependent hopping ground state expectation value

Furthermore one defines the  $\mathbf{r}$  dependent long-range hopping operator as

$$\hat{\Gamma}_{\mathbf{r},c,\sigma} = \frac{1}{N_{sit}} \sum_{\mathbf{j}} (\hat{c}_{\mathbf{j},\sigma}^\dagger \hat{c}_{\mathbf{j}+\mathbf{r},\sigma} + \hat{c}_{\mathbf{j}+\mathbf{r},\sigma}^\dagger \hat{c}_{\mathbf{j},\sigma}), \quad (11)$$

where, on the background of periodic boundary conditions in both directions,  $\sum_{\mathbf{j}}$  runs over all sites,  $c = d, f$ , and  $\sigma$  is an arbitrary spin projection. The calculations again are performed in  $\mathbf{k}$  space, and calculation details are also contained in Appendix C: the  $\mathbf{k}$  space expression of (11) is given in (C7), while its ground state expectation value is exemplified in (C8). The results are presented in Fig. 5. which exemplifies the d-electron behaviour in  $\mathbf{x}$  direction. As seen,  $\Gamma_{\mathbf{r}}$  increases if the effective total spin-orbit interaction  $\lambda = (1/2) \sum_{c=d,f} \lambda_c$  increases. Since  $\Gamma_{\mathbf{r}}$  is related to the hopping probability, the result presented in Fig.5 shows that the mobility of carriers increases with the spin-orbit interaction, and that the hopping probability (hence mobility) for the spin projection in the direction of the spontaneous magnetisation is at least five times higher than the hopping probability for the opposed spin direction.

## C. Observation relating the obtained solution

First one notes that using the  $N > N^*$  ground state (9) in deducing the ground state expectation values, the results presented in this section remain qualitatively unchanged:  $\bar{S}^z \neq 0$ , and with the observation that the  $\mathbf{r}$  dependent hopping  $\Gamma_{\mathbf{r}}$  substantially increases for higher distances, the information contained in Figs.4-5 qualitatively remains true.

The second aspect which we must mention, is that the obtained exact results are connected to a non-integrable system, hence as always in this case<sup>40</sup>, they are linked to a restricted region of the parameter space built up from the coupling constants and physical parameters of the Hamiltonian. This is because the matching system of equations providing the explicit expression of the block operator parameters, also leads to interconnections in between Hamiltonian parameters [see Appendix A, e.g. (A15)]. These interconnections define the restricted parameter space region in which the solution is valid. Here we would like to present this region.

We have in the model (besides the on-site one particle potentials and local hybridizations) only nearest-neighbor hoppings and hybridizations in the kinetic part of the Hamiltonian.

Without spin-flip hopping terms (i.e. spin-orbit interaction), all Hamiltonian parameters with opposite spin indices are equal (i.e.  $W_{\mathbf{p}}^{c,c',\alpha,\alpha} = W_{\mathbf{p}}^{c,c',-\alpha,-\alpha} = W_{\mathbf{p}}^{c,c'}$ , where  $W = t, V$ , so represents hoppings (in this case  $c = c'$ ), or hybridizations (in this case  $c \neq c'$  as well,  $c, c' = d, f$ ), and one has  $\mathbf{p} = \mathbf{x}, \mathbf{y}, 0$ . Furthermore, taking contributions from the two bands,  $d, f$ , relating  $W$  one observes that the matching system of equations provides the relation

$$W_{\mathbf{p}}^{c,c'} = w^{\delta_{d,c} + \delta_{d,c'}} W_{\mathbf{p}}^{f,f}, \quad (12)$$

where  $w = |u/v|$  is a constant. Such type of relations are effectively observed in two-band systems<sup>55</sup>, hence often used during theoretical descriptions<sup>41</sup>, consequently do not represent unrealistic restrictions. We note that also the second equality from (A24) enters in the category of the relation (12), because it can be written as  $k_1 V_{\mathbf{x}}^{c=d,c'=f,\alpha,\alpha} = w t_{\mathbf{x}}^{f,f,\alpha,-\alpha}$ , where the new, strongly reductive factor  $k_1$  emerges because of the spin change  $-\alpha \rightarrow \alpha$ . If for a concrete system under study is necessary to accomodate  $t_{\mathbf{x}}^{f,f,\alpha,-\alpha}$  to this equality, one notes that external electrical potential gradient at the surface can be used<sup>8</sup> to modify the effective spin-orbit interaction value.

The following observation relates the spin-flip hopping terms for which the matching equations require a relation of the type (12), but with minus sign [see (A16)]. We underline, that these requirements are also realistic. In order to show this we mention that calculating separately the d and f contributions to the total  $\hat{S}^z$  ground state expectation value, one finds that  $\langle \hat{S}_d^z \rangle$  and  $\langle \hat{S}_f^z \rangle$  do not coincide in sign. Since the f-carriers experience the Hubbard repulsion, they are the *heavier* particles while the d-carriers are the *light* particles in the system. But one knows that in two band systems the light carriers often try to compensate partially the heavier particle spin moments as one encounters this effect in the case of the periodic Anderson model as well<sup>56,57</sup>. Consequently, since the d and f spin orientations in average are opposed, the source term of the spin-orbit interaction<sup>51</sup>  $\vec{\sigma} \cdot (\nabla V \times \vec{p})$ , where  $\vec{\sigma}$  is the spin orientation, changes sign. This means that the spin-flip hopping terms change sign if one changes the particle type index f to d.

The last restrictive relation is the first equality of (A24) which provides a requirement for the value of the local hybridization. But one knows that the local hybridization can be modified by the concentration of the impurities on the surface<sup>58</sup>, hence this requirement can be experimentally satisfied. Interestingly, this requirement relating the local hybridization can be also enrolled on the line of (12), since can be written as  $k_2 k_1 V_{\mathbf{p}'=0}^{c=d,c'=f,\alpha,\alpha} = w t_{\mathbf{p}=\mathbf{x}}^{f,f,\alpha,-\alpha}$ ,

where the second correction factor  $k_2$  emerges because of the  $\mathbf{p}$  index change  $\mathbf{x} \rightarrow 0$ .

Concluding this subsection, as was presented above, the requirements characterizing the restricted parameter space region can be experimentally easily fulfilled.

## VII. SUMMARY AND CONCLUSIONS

A two-bands system has been analysed on a square 2D Bravais lattice possessing a correlated band holding on-site Coulomb repulsion, hybridized with a non-correlated band, in the presence of many-body spin-orbit interactions. Even if the system is non-integrable, exact many-body ground states have been deduced for it in the high concentration limit using a technique based on Positive Semidefinite Operator properties. For this to be possible, block operators holding both spin projections have been used, and at the transformation of the system Hamiltonian in a positive semidefinite form, solution has been provided for the matching system of equations containing 74 coupled, non-linear complex-algebraic equations. In our knowledge, other exact results for interacting many-body 2D systems in the presence of spin-orbit interactions are not present in the literature. The studied ground state being strongly entangled is ferromagnetic and presents (differentiated for different spin projections) an enhanced mobility of carriers. The increasing effective spin-orbit interaction in the correlated band increases the magnetisation, while the total effective spin-orbit interaction from both bands increases the  $\mathbf{r}$  dependent hopping ground state expectation value enhancing the mobility of carriers. The hopping probability for spin projection in the direction of the spontaneous magnetisation is at least five times higher than the hopping probability for the opposed spin projection. Based on the deduced results the emergence of ferromagnetic interfaces in between non-magnetic but strongly correlated materials could be in principle explained based on the presence of the spin-orbit interaction at the interface. Since strong mobility increase is observed for a given spin projection, applications in spintronics become possible.

## Acknowledgements

N. K. acknowledges the support of UNKP-17-2 New National Excellence Program of the Hungarian Ministry of Human Capacities, while Z. G. acknowledges the support of

the project NKFI-128018 of Hungarian funds for basic research and of the Alexander von Humboldt Foundation.

## Appendix A: The matching equations

### 1. The system of matching equations

For more visibility one introduces the notations  $g_{G=A,c,n,\alpha} = a_{n,c,\alpha}$ , and  $g_{G=B,c,n,\alpha} = b_{n,c,\alpha}$ . Using these notations, the matching equations become as follows:

#### *a. Matching equations from hopping contributions*

The first 32 matching equations are related to the hopping contributions. In these equations everywhere one has  $c = d, f$ , and  $(\alpha, \alpha') = (\uparrow, \uparrow); (\downarrow, \downarrow); (\uparrow, \downarrow); (\downarrow, \uparrow)$ .

i) The first 8 equations are related to the nearest-neighbor hopping terms in  $\mathbf{x}$  direction

$$-t_{\mathbf{x}}^{c,\alpha,\alpha'} = a_{2,c,\alpha}^* a_{1,c,\alpha'} + a_{3,c,\alpha}^* a_{4,c,\alpha'} + b_{2,c,\alpha}^* b_{1,c,\alpha'} + b_{3,c,\alpha}^* b_{4,c,\alpha'}. \quad (\text{A1})$$

ii) Similarly, the second 8 equations are related to the nearest-neighbor hopping terms in  $\mathbf{y}$  direction

$$-t_{\mathbf{y}}^{c,\alpha,\alpha'} = a_{4,c,\alpha}^* a_{1,c,\alpha'} + a_{3,c,\alpha}^* a_{2,c,\alpha'} + b_{4,c,\alpha}^* b_{1,c,\alpha'} + b_{3,c,\alpha}^* b_{2,c,\alpha'}. \quad (\text{A2})$$

iii) The next nearest-neighbor hoppings (missing from the starting  $\hat{H}$  from (3)) in  $\mathbf{y} + \mathbf{x}$  direction give the following 8 homogeneous equations

$$-t_{\mathbf{y}+\mathbf{x}}^{c,\alpha,\alpha'} = 0 = a_{3,c,\alpha}^* a_{1,c,\alpha'} + b_{3,c,\alpha}^* b_{1,c,\alpha'}. \quad (\text{A3})$$

iv) The last 8 equations from this group are related again to next nearest-neighbor hoppings missing from the starting  $\hat{H}$  from (3). These hoppings are in  $\mathbf{y} - \mathbf{x}$  direction and provide again homogeneous equations

$$-t_{\mathbf{y}-\mathbf{x}}^{c,\alpha,\alpha'} = 0 = a_{4,c,\alpha}^* a_{2,c,\alpha'} + b_{4,c,\alpha}^* b_{2,c,\alpha'}. \quad (\text{A4})$$

*b. Matching equations from non-local hybridizations*

The second 32 matching equations are related to the non-local hybridizations. For all these equations one has  $(c, c') = (d, f); (f, d)$ , and  $(\alpha, \alpha') = (\uparrow, \uparrow); (\downarrow, \downarrow); (\uparrow, \downarrow); (\downarrow, \uparrow)$ .

i) The first 8 equations from this group are related to the non-local hybridizations in  $\mathbf{x}$  direction

$$-V_{\mathbf{x}}^{c,c',\alpha,\alpha'} = a_{2,c,\alpha}^* a_{1,c',\alpha'} + a_{3,c,\alpha}^* a_{4,c',\alpha'} + b_{2,c,\alpha}^* b_{1,c',\alpha'} + b_{3,c,\alpha}^* b_{4,c',\alpha'}. \quad (\text{A5})$$

ii) The second 8 equations from this group are similarly related to the non-local hybridizations in  $\mathbf{y}$  direction

$$-V_{\mathbf{y}}^{c,c',\alpha,\alpha'} = a_{4,c,\alpha}^* a_{1,c',\alpha'} + a_{3,c,\alpha}^* a_{2,c',\alpha'} + b_{4,c,\alpha}^* b_{1,c',\alpha'} + b_{3,c,\alpha}^* b_{2,c',\alpha'}. \quad (\text{A6})$$

iii) As in the hopping case, for the next nearest-neighbor hybridizations in  $\mathbf{y} + \mathbf{x}$  direction, missing from the starting Hamiltonian (3) one obtain 8 homogeneous equations

$$-V_{\mathbf{y}+\mathbf{x}}^{c,c',\alpha,\alpha'} = 0 = a_{3,c,\alpha}^* a_{1,c',\alpha'} + b_{3,c,\alpha}^* b_{1,c',\alpha'}. \quad (\text{A7})$$

iv) Finally, for the next nearest-neighbor hybridizations in  $\mathbf{y} - \mathbf{x}$  direction, again missing from the starting  $\hat{H}$  in (3), we obtain the last 8 homogeneous equations from this group, namely

$$-V_{\mathbf{y}-\mathbf{x}}^{c,c',\alpha,\alpha'} = 0 = a_{4,c,\alpha}^* a_{2,c',\alpha'} + b_{4,c,\alpha}^* b_{2,c',\alpha'}. \quad (\text{A8})$$

*c. Matching equations from local hybridizations*

Since according to the second equality from (1) one has  $V_0^{d,f,\alpha,\alpha'} = (V_0^{f,d,\alpha',\alpha})^*$ , the local hybridizations provide only 4 matching equations. These written for  $(c, c') = (d, f)$  and  $(\alpha, \alpha') = (\uparrow, \uparrow); (\downarrow, \downarrow); (\uparrow, \downarrow); (\downarrow, \uparrow)$ , give the following relation

$$-V_0^{d,f,\alpha,\alpha'} = \sum_{n=1}^4 (a_{n,d,\alpha}^* a_{n,f,\alpha'} + b_{n,d,\alpha}^* b_{n,f,\alpha'}). \quad (\text{A9})$$

*d. Matching equations from local one-particle potentials*

In the case of local one-particle potentials, given by (1) one has for each  $c = d, f$  the equality  $\epsilon_c^{\uparrow,\downarrow} = (\epsilon_c^{\downarrow,\uparrow})^*$ , hence for a fixed  $c$  index, three matching equations appear. Consequently, for  $\epsilon_c^{\alpha,\alpha'}$  at  $c = d, f$  one has 6 matching equations, namely, for  $\alpha = \alpha' = \uparrow, \downarrow$ , in total



4 equations (note that here  $U_d = 0$ )

$$\epsilon_c^{\alpha,\alpha} + U_c - \eta = \sum_{n=1}^4 (a_{n,c,\alpha}^* a_{n,c,\alpha} + b_{n,c,\alpha}^* b_{n,c,\alpha}), \quad (\text{A10})$$

while for  $\alpha = \uparrow, \alpha' = \downarrow$  and  $c = d, f$ , in total 2 equations

$$\epsilon_c^{\uparrow,\downarrow} = \sum_{n=1}^4 (a_{n,c,\uparrow}^* a_{n,c,\downarrow} + b_{n,c,\uparrow}^* b_{n,c,\downarrow}). \quad (\text{A11})$$

Note that the total number of matching equations obtained (A1 - A11) is 74.

## 2. The solution of matching system of equations

### a. The first group of 42 equations

#### The next nearest neighbor contributions

The unknown variables of the matching equations are the  $a_{n,c,\alpha}, b_{n,c,\alpha}$  numerical prefactors that must be expressed in function of the physical parameters of the starting Hamiltonian. The solution process in the first step treats the 32 homogeneous equations (A3,A4,A7,A8) which provides the expression of all  $a_{n,c,\alpha}$  coefficients in function of  $b_{n,c,\alpha}$  coefficients as follows. For both indices  $\alpha = \uparrow, \downarrow$ , and both  $c = d, f$  one has

$$a_{1,c,\alpha} = -\frac{1}{x} b_{1,c,\alpha}, \quad a_{2,c,\alpha} = -\frac{1}{v} b_{2,c,\alpha}, \quad a_{3,c,\alpha} = x^* b_{3,c,\alpha}, \quad a_{4,c,\alpha} = v^* b_{4,c,\alpha}, \quad (\text{A12})$$

where  $x, v$  are at the moment arbitrary ( $\neq 0, \infty$ ) parameters. (A12) gives 16 relations based on which, all 32 homogeneous matching equations connected to next nearest neighbor hoppings and hybridizations with zero value are satisfied.

#### The spin-flip hybridization contributions

In the following step one analyzes the group of 10 equations related to non-local (8 equations) and local (2 equations) hybridization terms containing spin-flip, which are also missing from the starting Hamiltonian. In the case of non-local hybridizations, these contributions are present in (A5,A6) as  $V_{\mathbf{p}}^{c,c',\uparrow,\downarrow}, V_{\mathbf{p}}^{c,c',\downarrow,\uparrow}$ , with  $\mathbf{p} = \mathbf{x}, \mathbf{y}$ , and  $(c, c') = (d, f), (f, d)$ . In the case of local hybridizations, the discussed contributions are present in (A9) as  $V_0^{d,f,\uparrow,\downarrow}$  and  $V_0^{d,f,\downarrow,\uparrow}$ . All these equations allow the expression of  $b_{n,d,\alpha}$  prefactors in function of  $b_{n,f,\alpha}$  coefficients as follows

$$b_{1,d,\alpha} = \frac{x u_\alpha}{v} b_{3,f,-\alpha}^*, \quad b_{2,d,\alpha} = u_\alpha b_{4,f,-\alpha}^*, \quad b_{3,d,\alpha} = -\frac{u_\alpha}{x^* v} b_{1,f,-\alpha}^*, \quad b_{4,d,\alpha} = -\frac{u_\alpha}{|v|^2} b_{2,f,-\alpha}^*. \quad (\text{A13})$$

The equalities (A13) represent in total 8 relations. Here  $u_\alpha$ ,  $\alpha = \uparrow, \downarrow$  are at the moment arbitrary ( $\neq 0, \infty$ ) numerical parameters.

At this moment, from the matching relations only 32 equations remain [8 from (A1), 8 from (A2), 4 from (A5), 4 from (A6), 2 from (A9), 4 from (A10), and 2 from (A11)].

*b. The remaining group of 32 equations*

The 15 interdependent equations

From the remaining 32 equations, 17 are linearly independent, and 15 are dependent on these. In this subsection we analyse these last 15 interdependent relations. Taking  $u = u_\uparrow = -u_\downarrow$ , the interdependences provide i) spin projection independence for non-local hybridization parameters

$$V_{\mathbf{p}}^{c,c',\alpha,\alpha} = V_{\mathbf{p}}^{c,c',-\alpha,-\alpha}, \quad (\text{A14})$$

where  $(c, c') = (d, f); (f, d)$ , and  $\alpha = \uparrow, \downarrow$ , hence (A14) gives 4 equations; ii) preserves the spin projection independence possibility in hopping terms without spin-flip and fixes the magnitude ratio between d and f nearest-neighbor hoppings and d and f on-site one-particle potentials

$$t_{\mathbf{p}}^{d,\alpha,\alpha} = K t_{\mathbf{p}}^{f,\alpha,\alpha}, \quad \bar{\epsilon}_d^{\alpha,\alpha} = K \bar{\epsilon}_f^{\alpha,\alpha} \quad (\text{A15})$$

where  $\bar{\epsilon}_d = \epsilon_d - \eta$ ,  $\bar{\epsilon}_f = \epsilon_f + U_f - \eta$ , and  $K = |u/v|^2$ ,  $\mathbf{p} = \mathbf{x}, \mathbf{y}$  [note that (A15) means 6 relations], iii) fixes the magnitude ratio of the absolute values of d and f spin-flip hoppings to  $K$  as

$$t_{\mathbf{p}}^{d,\alpha,\alpha'} = -K t_{\mathbf{p}}^{f,\alpha,\alpha'}, \quad (\text{A16})$$

which represent 4 relations, and finally iv) fixes a proportionality in between  $\epsilon_d^{\uparrow,\downarrow}$  and  $\epsilon_f^{\uparrow,\downarrow}$  (1 relation)

$$\epsilon_d^{\uparrow,\downarrow} = \frac{u_\uparrow^* u_\downarrow}{|v|^2} \epsilon_f^{\uparrow,\downarrow}. \quad (\text{A17})$$

The equations (A14-A17) are the mentioned 15 interdependences.

The remaining 17 matching equations

From the remaining 17 matching equations first  $\epsilon_f^{\uparrow,\downarrow} = 0$  is taken, since this parameter is missing from the starting Hamiltonian in (3). This provides the possibility to express  $b_{n,f,\alpha}$  for  $n = 3, 4$  in function of the coefficients  $b_{m,f,\alpha}$  for  $m = 1, 2$  as follows

$$b_{3,f,\uparrow} = -\frac{1}{x^*}b_{1,f,\uparrow}e^{+i\phi_3}, \quad b_{3,f,\downarrow} = \frac{1}{x^*}b_{1,f,\downarrow}e^{+i\phi_3}, \quad b_{4,f,\uparrow} = -\frac{1}{v^*}b_{2,f,\uparrow}e^{+i\phi_4}, \quad b_{4,f,\downarrow} = \frac{1}{v^*}b_{2,f,\uparrow}e^{+i\phi_4} \quad (\text{A18})$$

where at the moment  $\phi_3, \phi_4$  are arbitrary phases. Note that at this step 16 matching equations remain. 5 equations from these give the following equalities

$$\begin{aligned} V_0^{d,f,\downarrow,\downarrow} &= V_0^{d,f,\uparrow,\uparrow}, \quad t_{\mathbf{y}}^{f,\uparrow,\downarrow} = \frac{v-x}{1+xv^*} \frac{v^*}{v} e^{-i\phi_4} t_{\mathbf{x}}^{f,\uparrow,\downarrow}, \quad t_{\mathbf{y}}^{f,\downarrow,\uparrow} = -\frac{v-x}{1+xv^*} \frac{v^*}{v} e^{-i\phi_4} t_{\mathbf{x}}^{f,\downarrow,\uparrow}, \\ (V_{\mathbf{x}}^{f,d,\uparrow,\uparrow})^* &= e^{2i\theta_1} e^{i(\phi_3-\phi_4)} V_{\mathbf{x}}^{d,f,\uparrow,\uparrow}, \quad (V_{\mathbf{y}}^{f,d,\uparrow,\uparrow})^* = -e^{2i\theta_2} e^{i(\phi_3+\phi_4)} V_{\mathbf{y}}^{d,f,\uparrow,\uparrow}, \end{aligned} \quad (\text{A19})$$

where  $\theta_1$  is the phase of  $Q_1 = \frac{xv^*}{1+xv^*}$ , and  $\theta_2$  is the phase of  $Q_2 = \frac{xv}{x-v}$ . The remaining 11 matching equations are presented below:

The remaining 11 matching equations

$$\begin{aligned} -t_{\mathbf{x}}^{f,\uparrow,\uparrow} &= (1 + \frac{1}{xv^*})(b_{2,f,\uparrow}^* b_{1,f,\uparrow} + e^{i(\phi_4-\phi_3)} b_{1,f,\uparrow}^* b_{2,f,\uparrow}), \\ -t_{\mathbf{x}}^{f,\downarrow,\downarrow} &= (1 + \frac{1}{xv^*})(b_{2,f,\downarrow}^* b_{1,f,\downarrow} + e^{i(\phi_4-\phi_3)} b_{1,f,\downarrow}^* b_{2,f,\downarrow}), \\ -t_{\mathbf{x}}^{f,\uparrow,\downarrow} &= (1 + \frac{1}{xv^*})(b_{2,f,\uparrow}^* b_{1,f,\downarrow} - e^{i(\phi_4-\phi_3)} b_{1,f,\uparrow}^* b_{2,f,\downarrow}), \\ -t_{\mathbf{x}}^{f,\downarrow,\uparrow} &= (1 + \frac{1}{xv^*})(b_{2,f,\downarrow}^* b_{1,f,\uparrow} - e^{i(\phi_4-\phi_3)} b_{1,f,\downarrow}^* b_{2,f,\uparrow}), \\ -t_{\mathbf{y}}^{f,\uparrow,\uparrow} &= \frac{v-x}{xv} e^{-i\phi_4} (b_{2,f,\uparrow}^* b_{1,f,\uparrow} - e^{i(\phi_4-\phi_3)} b_{1,f,\uparrow}^* b_{2,f,\uparrow}), \\ -t_{\mathbf{y}}^{f,\downarrow,\downarrow} &= \frac{x-v}{xv} e^{-i\phi_4} (b_{2,f,\downarrow}^* b_{1,f,\downarrow} - e^{i(\phi_4-\phi_3)} b_{1,f,\downarrow}^* b_{2,f,\downarrow}), \\ -V_{\mathbf{x}}^{d,f,\uparrow,\uparrow} &= \frac{1+xv^*}{xv^*} (\frac{u}{v})^* e^{i\phi_4} (b_{1,f,\uparrow} b_{2,f,\downarrow} + b_{1,f,\downarrow} b_{2,f,\uparrow}), \\ -V_{\mathbf{y}}^{d,f,\uparrow,\uparrow} &= \frac{v-x}{xv} (\frac{u}{v})^* (b_{1,f,\uparrow} b_{2,f,\downarrow} - b_{1,f,\downarrow} b_{2,f,\uparrow}), \\ -V_0^{d,f,\uparrow,\uparrow} &= 2(\frac{u}{v})^* [(1 + \frac{1}{|x|^2}) e^{i\phi_3} b_{1,f,\uparrow} b_{1,f,\downarrow} + (1 + \frac{1}{|v|^2}) e^{i\phi_4} b_{2,f,\uparrow} b_{2,f,\downarrow}], \\ \bar{\epsilon}_f^{\uparrow,\uparrow} &= 2[(1 + \frac{1}{|x|^2}) |b_{1,f,\uparrow}|^2 + (1 + \frac{1}{|v|^2}) |b_{2,f,\uparrow}|^2], \\ \bar{\epsilon}_f^{\downarrow,\downarrow} &= 2[(1 + \frac{1}{|x|^2}) |b_{1,f,\downarrow}|^2 + (1 + \frac{1}{|v|^2}) |b_{2,f,\downarrow}|^2]. \end{aligned} \quad (\text{A20})$$

Now, since from (4) at  $\mathbf{p} = \mathbf{x}$ , the spin-flip hopping terms must satisfy  $t_{\mathbf{x}}^{c,\downarrow,\uparrow} = -(t_{\mathbf{x}}^{c,\uparrow,\downarrow})^*$ , from the third and fourth equality of (A20) one finds  $\theta_1 = 0, \phi_3 = \phi_4$ . After this step one can see from (A20) that  $t_{\mathbf{x}}^{f,\uparrow,\uparrow} = t_{\mathbf{x}}^{f,\downarrow,\downarrow}$ , and  $t_{\mathbf{y}}^{f,\uparrow,\uparrow} = t_{\mathbf{y}}^{f,\downarrow,\downarrow}$  are satisfied by

$$b_{2,f,\downarrow} = \frac{b_{2,f,\uparrow}^* b_{1,f,\uparrow}}{b_{1,f,\downarrow}^*}, \quad (\text{A21})$$

and one remains from (A20) with 8 matching equations. Given by (4,A19) which require the same absolute value for  $t_y^{f,\uparrow,\downarrow}$  and  $t_x^{f,\uparrow,\downarrow}$  one must has  $(v-x)/(1+xv^*) = z$  with  $|z| = 1$ , which provide for  $v = |v|e^{i\phi_v}$  the expression  $x = |x|e^{i\phi_v}$ , where  $|x| = (|v| - 1)/(|v| + 1)$ , and  $\theta_2 = \phi_v$  holds. Now the last two equalities from (A20) via  $\bar{\epsilon}_f^{\uparrow,\uparrow} = \bar{\epsilon}_f^{\downarrow,\downarrow}$ , and the choise  $t_x^{f,\uparrow,\downarrow} \neq 0$  give

$$b_{2,f,\uparrow} = \frac{|v|\sqrt{2}}{|(|v| - 1)|} b_{1,f,\downarrow} e^{i\gamma}, \quad b_{2,f,\downarrow} = \frac{|v|\sqrt{2}}{|(|v| - 1)|} b_{1,f,\uparrow} e^{-i\gamma}, \quad (\text{A22})$$

where  $\gamma$  is an arbitrary phase, one can express  $\eta$  via  $\bar{\epsilon}_f^{\uparrow,\uparrow}$  as

$$\eta = \epsilon_f^{\uparrow,\uparrow} + U_f - 4 \frac{(1 + |v|^2)}{(|v| - 1)^2} (|b_{1,f,\downarrow}|^2 + |b_{1,f,\uparrow}|^2), \quad (\text{A23})$$

and  $V_0^{d,f,\uparrow,\uparrow}$ , and  $t_x^{f,\uparrow,\downarrow}$  respectively become

$$\begin{aligned} -V_0^{d,f,\uparrow,\uparrow} &= 8e^{i\chi} \frac{u^*}{|v|} \frac{(1 + |v|^2)}{(1 - |v|)^2} b_{1,f,\uparrow} b_{1,f,\downarrow}, \\ -t_x^{f,\uparrow,\downarrow} &= \frac{\sqrt{2}(1 + |v|^2)}{(|v| - 1)^2} e^{-i\gamma} (|b_{1,f,\downarrow}|^2 - |b_{1,f,\uparrow}|^2). \end{aligned} \quad (\text{A24})$$

At this step one remains from (A20) with 4 matching equations (those related to  $t_p^{f,\uparrow,\uparrow}$  and  $V_p^{d,f,\uparrow,\uparrow}$  for  $p = x, y$ , i.e. 1th, 5th, 7th, 8th equalities), which must be used in deducing the last two unknown block operator parameters  $b_{1,f,\uparrow}$ , and  $b_{1,f,\downarrow}$ .

#### The remaining last 4 matching equations

Using now the 7th and 8th equation from (A20) and the notations

$$\begin{aligned} -(V_x^{d,f,\uparrow,\uparrow} e^{-i\chi} + V_y^{d,f,\uparrow,\uparrow}) &= \Theta_{\uparrow} e^{i\delta_{\uparrow}}, \quad \Theta_{\uparrow} = |V_x^{d,f,\uparrow,\uparrow} e^{-i\chi} + V_y^{d,f,\uparrow,\uparrow}|, \\ -(V_x^{d,f,\uparrow,\uparrow} e^{-i\chi} - V_y^{d,f,\uparrow,\uparrow}) &= \Theta_{\downarrow} e^{i\delta_{\downarrow}}, \quad \Theta_{\downarrow} = |V_x^{d,f,\uparrow,\uparrow} e^{-i\chi} - V_y^{d,f,\uparrow,\uparrow}|, \end{aligned} \quad (\text{A25})$$

one finds

$$\begin{aligned} b_{1,f,\uparrow} &= \sqrt{\frac{(|v| - 1)^2}{2\sqrt{2}(1 + |v|^2)} \frac{|v|}{|u|}} \sqrt{\Theta_{\uparrow}} e^{i(\gamma + \phi_u + \delta_{\uparrow})/2}, \\ b_{1,f,\downarrow} &= \sqrt{\frac{(|v| - 1)^2}{2\sqrt{2}(1 + |v|^2)} \frac{|v|}{|u|}} \sqrt{\Theta_{\downarrow}} e^{i(-\gamma + \phi_u + \delta_{\downarrow})/2}, \end{aligned} \quad (\text{A26})$$

where  $\chi = \phi_3 + \phi_v$ . Finally, from the first and 5th equation of (A20), the  $|v|/|u|$  ratio and the  $(\delta_{\uparrow} - \delta_{\downarrow})$  phase (with the choise  $\chi = \pi/2$ ) can be expressed as

$$\frac{|v|}{|u|} = \frac{-t_x^{f,\uparrow,\uparrow}}{\sqrt{\Theta_{\uparrow}\Theta_{\downarrow}} \cos \frac{\delta_{\uparrow} - \delta_{\downarrow}}{2}}, \quad \tan \frac{\delta_{\uparrow} - \delta_{\downarrow}}{2} = \frac{t_y^{f,\uparrow,\uparrow}}{t_x^{f,\uparrow,\uparrow}}. \quad (\text{A27})$$

We underline that based on the presented solution, starting from (A26,A27) and using (A12,A13,A18,A22), all unknown block operator parameters can be explicitly expressed in function of Hamiltonian parameters.

## Appendix B: The kinetic Hamiltonian in $\mathbf{k}$ space

Transforming  $\hat{H}_{kin}$  from (3) in  $\mathbf{k}$  space via  $\hat{c}_{j,\sigma} = (1/\sqrt{N_{sit}}) \sum_{\mathbf{k}} \exp(-i\mathbf{kj}) \hat{c}_{\mathbf{k},\sigma}$ ,  $c = d, f$ , one obtains

$$\hat{H}_{kin} = \sum_{\mathbf{k}} \sum_{\sigma, \sigma'} [\epsilon_{d,\mathbf{k}}^{\sigma, \sigma'} \hat{d}_{\mathbf{k},\sigma}^\dagger \hat{d}_{\mathbf{k},\sigma'} + \epsilon_{f,\mathbf{k}}^{\sigma, \sigma'} \hat{f}_{\mathbf{k},\sigma}^\dagger \hat{f}_{\mathbf{k},\sigma'} + V_{d,f,\mathbf{k}}^{\sigma, \sigma'} \hat{d}_{\mathbf{k},\sigma}^\dagger \hat{f}_{\mathbf{k},\sigma'} + V_{d,f,\mathbf{k}}^{\sigma, \sigma'}^* \hat{f}_{\mathbf{k},\sigma}^\dagger \hat{d}_{\mathbf{k},\sigma'}]. \quad (\text{B1})$$

Introducing the column vector  $\mathbf{v}$ , its transpose conjugate (the row vector  $\mathbf{v}^\dagger$ ), and the matrix  $\tilde{W}$  as

$$\mathbf{v} = \begin{pmatrix} \hat{d}_{\mathbf{k},\uparrow} \\ \hat{f}_{\mathbf{k},\uparrow} \\ \hat{d}_{\mathbf{k},\downarrow} \\ \hat{f}_{\mathbf{k},\downarrow} \end{pmatrix}, \quad \mathbf{v}^\dagger = (\hat{d}_{\mathbf{k},\uparrow}^\dagger, \hat{f}_{\mathbf{k},\uparrow}^\dagger, \hat{d}_{\mathbf{k},\downarrow}^\dagger, \hat{f}_{\mathbf{k},\downarrow}^\dagger), \quad \tilde{W} = \begin{pmatrix} \epsilon_{d,\mathbf{k}}^{\uparrow,\uparrow} & V_{d,f,\mathbf{k}}^{\uparrow,\uparrow} & \epsilon_{d,\mathbf{k}}^{\uparrow,\downarrow} & 0 \\ V_{d,f,\mathbf{k}}^{\uparrow,\uparrow *} & \epsilon_{f,\mathbf{k}}^{\uparrow,\uparrow} & 0 & \epsilon_{f,\mathbf{k}}^{\uparrow,\downarrow} \\ \epsilon_{d,\mathbf{k}}^{\uparrow,\downarrow *} & 0 & \epsilon_{d,\mathbf{k}}^{\downarrow,\downarrow} & V_{d,f,\mathbf{k}}^{\downarrow,\downarrow} \\ 0 & \epsilon_{f,\mathbf{k}}^{\uparrow,\downarrow *} & V_{d,f,\mathbf{k}}^{\downarrow,\downarrow *} & \epsilon_{f,\mathbf{k}}^{\downarrow,\downarrow} \end{pmatrix}, \quad (\text{B2})$$

one finds

$$\hat{H}_{kin} = \sum_{\mathbf{k}} (\hat{d}_{\mathbf{k},\uparrow}^\dagger, \hat{f}_{\mathbf{k},\uparrow}^\dagger, \hat{d}_{\mathbf{k},\downarrow}^\dagger, \hat{f}_{\mathbf{k},\downarrow}^\dagger) \tilde{W} \begin{pmatrix} \hat{d}_{\mathbf{k},\uparrow} \\ \hat{f}_{\mathbf{k},\uparrow} \\ \hat{d}_{\mathbf{k},\downarrow} \\ \hat{f}_{\mathbf{k},\downarrow} \end{pmatrix} = \sum_{\mathbf{k}} \mathbf{v}^\dagger \tilde{W} \mathbf{v}, \quad (\text{B3})$$

where one has for  $c = d, f$  and  $\sigma, \sigma'$  the expressions

$$\begin{aligned} \epsilon_{c,\mathbf{k}}^{\sigma, \sigma'} &= \epsilon_c^{\sigma, \sigma'} + [t_x^{c,\sigma, \sigma'} e^{+i\mathbf{kx}} + (t_x^{c,\sigma', \sigma})^* e^{-i\mathbf{kx}}] + [t_y^{c,\sigma, \sigma'} e^{+i\mathbf{ky}} + (t_y^{c,\sigma', \sigma})^* e^{-i\mathbf{ky}}], \\ V_{d,f,\mathbf{k}}^{\sigma, \sigma'} &= V_0^{d,f,\sigma, \sigma'} + [V_x^{d,f,\sigma, \sigma'} e^{+i\mathbf{kx}} + (V_x^{f,d,\sigma', \sigma})^* e^{-i\mathbf{kx}}] + [V_y^{d,f,\sigma, \sigma'} e^{+i\mathbf{ky}} + (V_y^{f,d,\sigma', \sigma})^* e^{-i\mathbf{ky}}]. \end{aligned} \quad (\text{B4})$$

Note that the eigenvalue spectrum (i.e. the band structure) of  $\hat{H}_{kin}$  is obtained from the secular equation of  $\tilde{W}$ .

### Appendix C: Expectation values calculated with the ground state in $\mathbf{k}$ space

Transformed in  $\mathbf{k}$  space based on Appendix B, the ground state (8), in unnormalized form becomes

$$|\Psi_g\rangle = \prod_{\mathbf{k}} [\gamma_{1,\mathbf{k}} \hat{d}_{\mathbf{k},\uparrow}^\dagger \hat{d}_{\mathbf{k},\downarrow}^\dagger \hat{f}_{\mathbf{k},\uparrow}^\dagger + \gamma_{2,\mathbf{k}} \hat{d}_{\mathbf{k},\uparrow}^\dagger \hat{d}_{\mathbf{k},\downarrow}^\dagger \hat{f}_{\mathbf{k},\downarrow}^\dagger + \gamma_{3,\mathbf{k}} \hat{d}_{\mathbf{k},\uparrow}^\dagger \hat{f}_{\mathbf{k},\uparrow}^\dagger \hat{f}_{\mathbf{k},\downarrow}^\dagger + \gamma_{4,\mathbf{k}} \hat{d}_{\mathbf{k},\downarrow}^\dagger \hat{f}_{\mathbf{k},\uparrow}^\dagger \hat{f}_{\mathbf{k},\downarrow}^\dagger] |0\rangle. \quad (\text{C1})$$

Here and hereafter, all  $\sum_{\mathbf{k}}, \prod_{\mathbf{k}}$  extend over the first Brillouin zone. Furthermore, one has

$$\begin{aligned} \gamma_{1,\mathbf{k}} &= \gamma_{\uparrow}(a_{\mathbf{k},d,\uparrow}^* b_{\mathbf{k},d,\downarrow}^* - a_{\mathbf{k},d,\downarrow}^* b_{\mathbf{k},d,\uparrow}^*), & \gamma_{2,\mathbf{k}} &= \gamma_{\downarrow}(a_{\mathbf{k},d,\uparrow}^* b_{\mathbf{k},d,\downarrow}^* - a_{\mathbf{k},d,\downarrow}^* b_{\mathbf{k},d,\uparrow}^*), \\ \gamma_{3,\mathbf{k}} &= \gamma_{\downarrow}(a_{\mathbf{k},d,\uparrow}^* b_{\mathbf{k},f,\uparrow}^* - a_{\mathbf{k},f,\uparrow}^* b_{\mathbf{k},d,\uparrow}^*) - \gamma_{\uparrow}(a_{\mathbf{k},d,\uparrow}^* b_{\mathbf{k},f,\downarrow}^* - a_{\mathbf{k},f,\downarrow}^* b_{\mathbf{k},d,\uparrow}^*), \\ \gamma_{4,\mathbf{k}} &= \gamma_{\downarrow}(a_{\mathbf{k},d,\downarrow}^* b_{\mathbf{k},f,\uparrow}^* - a_{\mathbf{k},f,\uparrow}^* b_{\mathbf{k},d,\downarrow}^*) - \gamma_{\uparrow}(a_{\mathbf{k},d,\downarrow}^* b_{\mathbf{k},f,\downarrow}^* - a_{\mathbf{k},f,\downarrow}^* b_{\mathbf{k},d,\downarrow}^*). \end{aligned} \quad (\text{C2})$$

The connection between the block operator coefficients  $g_{G,c,n,\alpha}$  (see (6)), where  $g=a,b$  for  $G=A,B$ , furthermore  $c=d,f$ ;  $\alpha = \uparrow, \downarrow$ ;  $n=1,2,3,4$ ; and  $g_{G,\mathbf{k},c,\alpha}$  with  $g=a,b$  for  $G=A,B$  and  $c=d,f$ , is given by

$$g_{\mathbf{k},c,\alpha} = g_{G,c,1,\alpha} + g_{G,c,2,\alpha} e^{-i\mathbf{k}\mathbf{x}} + g_{G,c,3,\alpha} e^{-i\mathbf{k}(\mathbf{x}+\mathbf{y})} + g_{G,c,4,\alpha} e^{-i\mathbf{k}\mathbf{y}}, \quad (\text{C3})$$

see for notations also the first row of Appendix A, e.g.  $a_{\mathbf{k},d,\alpha} = a_{1,d,\alpha} + a_{2,d,\alpha} \exp(-i\mathbf{k}\mathbf{x}) + a_{2,d,\alpha} \exp[-i\mathbf{k}(\mathbf{x}+\mathbf{y})] + a_{4,d,\alpha} \exp(-i\mathbf{k}\mathbf{y})$ , etc. Starting from (C1) the norm becomes

$$\langle \Psi_g | \Psi_g \rangle = \prod_{\mathbf{k}} \left[ \sum_{n=1}^4 |\gamma_{n,\mathbf{k}}|^2 \right]. \quad (\text{C4})$$

Using now the total z-spin component operator from (10), and applying the relations

$$\begin{aligned} \langle \Psi_g | \hat{n}_{\mathbf{k},\uparrow}^d | \Psi_g \rangle &= |\gamma_{1,\mathbf{k}}|^2 + |\gamma_{2,\mathbf{k}}|^2 + |\gamma_{3,\mathbf{k}}|^2, & \langle \Psi_g | \hat{n}_{\mathbf{k},\downarrow}^d | \Psi_g \rangle &= |\gamma_{1,\mathbf{k}}|^2 + |\gamma_{2,\mathbf{k}}|^2 + |\gamma_{4,\mathbf{k}}|^2, \\ \langle \Psi_g | \hat{n}_{\mathbf{k},\uparrow}^f | \Psi_g \rangle &= |\gamma_{1,\mathbf{k}}|^2 + |\gamma_{3,\mathbf{k}}|^2 + |\gamma_{4,\mathbf{k}}|^2, & \langle \Psi_g | \hat{n}_{\mathbf{k},\downarrow}^f | \Psi_g \rangle &= |\gamma_{2,\mathbf{k}}|^2 + |\gamma_{3,\mathbf{k}}|^2 + |\gamma_{4,\mathbf{k}}|^2, \end{aligned} \quad (\text{C5})$$

one finds for the ground state expectation value of  $\hat{S}^z$  per site the expression

$$\frac{\langle \hat{S}^z \rangle}{N_{\text{sit}}} = \frac{1}{2N_{\text{sit}}} \sum_{\mathbf{k}} \frac{|\gamma_{3,\mathbf{k}}|^2 - |\gamma_{4,\mathbf{k}}|^2 + |\gamma_{1,\mathbf{k}}|^2 - |\gamma_{2,\mathbf{k}}|^2}{|\gamma_{1,\mathbf{k}}|^2 + |\gamma_{2,\mathbf{k}}|^2 + |\gamma_{3,\mathbf{k}}|^2 + |\gamma_{4,\mathbf{k}}|^2}. \quad (\text{C6})$$

Furthermore the  $\mathbf{r}$  dependent long-range hopping operator presented in (11) transformed in  $\mathbf{k}$  space becomes

$$\hat{\Gamma}_{\mathbf{r},c,\sigma} = \frac{2}{N_{\text{sit}}} \sum_{\mathbf{k}} \cos(\mathbf{k}\mathbf{r}) \hat{n}_{\mathbf{k},\sigma}^c. \quad (\text{C7})$$

where  $\sum_{\mathbf{k}}$  runs over the first Brillouin zone. If one takes for example  $c = d$ , and  $\sigma = \uparrow$  in (C7), based on (C5) one finds

$$\Gamma_{\mathbf{r},d,\uparrow} = \langle \hat{\Gamma}_{\mathbf{r},d,\uparrow} \rangle = \frac{2}{N_{sit}} \sum_{\mathbf{k}} \cos(\mathbf{k}\mathbf{r}) \frac{\sum_{\alpha=1}^3 |\gamma_{\alpha,\mathbf{k}}|^2}{\sum_{\alpha=1}^4 |\gamma_{\alpha,\mathbf{k}}|^2}. \quad (\text{C8})$$

The  $\sum_{\mathbf{k}}$  in (C6,C8) can be effectuated in the thermodynamic limit by choosing the length units such to have the  $V_c = 1$  for the unit cell volume. In this case  $N_{sit} = V$ ,  $V$  being the sample's volume, and one has  $(1/V) \sum_{\mathbf{k}} = \int d^2\mathbf{k}/(2\pi)^2$ , where the integral must be taken on the first Brillouin zone. The calculations have been done in the case [see (8)]  $\gamma = \gamma_{\uparrow} = \gamma_{\downarrow}$ . At the first view this seems to be the most unfavorable case for ferromagnetism, but in fact the choice for  $\gamma_{\uparrow}, \gamma_{\downarrow}$  is equivalent in our case to a choice of the quantification z-axis, along which  $\langle \bar{S}^z \rangle$  is calculated.

- 
- <sup>1</sup> Yu. M. Koroteev, G. Bihlmayer, J. E. Gayone, E. V. Chulkov, S. Blgel, P. M. Echenique, and Ph. Hofmann, *Strong Spin-Orbit Splitting on Bi Surfaces*, Phys. Rev. Lett. 93 (2004), pp. 046403-1-046403-4. Available at <https://link.aps.org/doi/10.1103/PhysRevLett.93.046403>.
  - <sup>2</sup> C. R. Ast, J. Henk, A. Ernst, L. Moreschini, M. C. Falub, D. Pacil, P. Bruno, K. Kern, and M. Grioni, *Giant Spin Splitting through Surface Alloying*, Phys. Rev. Lett. 98 (2007), pp. 186807-1-186807-4. Available at <https://link.aps.org/doi/10.1103/PhysRevLett.98.186807>.
  - <sup>3</sup> M. B. Jungfleisch, W. Zhang, J. Sklenar, W. Jiang, J. E. Pearson, J. B. Ketterson, and A. Hoffmann, *Interface-driven spin-torque ferromagnetic resonance by Rashba coupling at the interface between nonmagnetic materials*, Phys. Rev. B 93 (2016), pp. 224419-1-224419-5. Available at <https://link.aps.org/doi/10.1103/PhysRevB.93.224419>.
  - <sup>4</sup> K. Yaji, Y. Ohtsubo, S. Hatta, H. Okuyama, K. Miyamoto, T. Okuda, A. Kimura, H. Namatame, M. Taniguchi, and T. Aruga, *Large Rashba spin splitting of a metallic surface-state band on a semiconductor surface*, Nature Commun. 1.2 (2010), pp. 1-5. Available at <https://www.ncbi.nlm.nih.gov/pmc/articles/PMC2909720/>.
  - <sup>5</sup> K. Sakamoto, H. Kakuta, K. Sugawara, K. Miyamoto, A. Kimura, T. Kuzumaki, N. Ueno, E. Annese, J. Fujii, A. Kodama, T. Shishidou, H. Namatame, M. Taniguchi, T. Sato, T. Takahashi, and T. Oguchi, *Peculiar Rashba splitting originating from the two-dimensional symmetry of the surface*, Phys. Rev. Lett. 103 (2009), pp. 156801-1-156801-4. Available at

- <https://link.aps.org/doi/10.1103/PhysRevLett.103.156801>.
- <sup>6</sup> K. Nakatsuji, R. Niikura, Y. Shibata, M. Yamada, T. Iimori, F. Komori, Y. Oda, and A. Ishii, *Anisotropic splitting and spin polarization of metallic bands due to spin-orbit interaction at the  $Ge(111)(\sqrt{3} \times \sqrt{3})R30^\circ$ -Au surface*, Phys. Rev. B84 (2011), pp. 035436-1-035436-4. Available at <https://link.aps.org/doi/10.1103/PhysRevB.84.035436>.
  - <sup>7</sup> P. Höpfner, J. Schäfer, A. Fleszar, J. H. Dil, B. Slomski, F. Meier, C. Loho, C. Blumenstein, L. Patthey, W. Hanke, and R. Claessen, *Three-Dimensional Spin Rotations at the Fermi Surface of a Strongly Spin-Orbit Coupled Surface System*, Phys. Rev. Lett. 108 (2012), pp. 186801-1-186801-5. Available at <https://link.aps.org/doi/10.1103/PhysRevLett.108.186801>.
  - <sup>8</sup> Q. F. Sun, J. Wang and H. Guo, *Quantum transport theory for nanostructures with Rashba spin-orbital interaction*, Phys. Rev. B71 (2005), pp. 165310-1-165310-11. Available at <https://link.aps.org/doi/10.1103/PhysRevB.71.165310>.
  - <sup>9</sup> S. Abdelouahed, A. Ernst, J. Henk, I. V. Maznichenko, and I. Mertig, *Spin-split electronic states in graphene: Effects due to lattice deformation, Rashba effect, and adatoms by first principles*, Phys. Rev. B82 (2010), pp. 125424-1-126424-8. Available at <https://link.aps.org/doi/10.1103/PhysRevB.82.125424>.
  - <sup>10</sup> M. I. Alomar and D. Sanchez, *Thermoelectric effects in graphene with local spin-orbit interaction*, Phys. Rev. B89 (2014), pp. 115422-1-115422-8. Available at <https://link.aps.org/doi/10.1103/PhysRevB.89.115422>.
  - <sup>11</sup> F. Mireles and G. Kirczenow, *Ballistic spin-polarized transport and Rashba spin precession in semiconductor nanowires*, Phys. Rev. B64 (2001), pp. 024426-1-024426-13. Available at <https://link.aps.org/doi/10.1103/PhysRevB.64.024426>.
  - <sup>12</sup> C. L. Kane and E. J. Mele,  *$Z_2$  Topological Order and the Quantum Spin Hall Effect*, Phys. Rev. Lett. 95 (2005), pp. 146802-1-146802-4. Available at <https://link.aps.org/doi/10.1103/PhysRevLett.95.146802>.
  - <sup>13</sup> A. Ohtomo and H. Y. Hwang, *A high-mobility electron gas at the  $LaAlO_3/SrTiO_3$  heterointerface*, Nature 427 (2004), pp. 423-426. Available at <http://dx.doi.org/10.1038/nature02308>.
  - <sup>14</sup> N. Reyren, S. Thiel, A. D. Caviglia, L. Kourkoutis, G. Hammerl, C. Richter, C. W. Schneider, T. Kopp, A.-S. Retschi, D. Jaccard, M. Gabay, D. A. Muller, J.-M. Triscone, and J. Mannhart, *Superconducting Interfaces Between Insulating Oxides*, Science 317 (2007), pp. 1196-1199. Available at <http://science.sciencemag.org/content/317/5842/1196.full.pdf>.



- <sup>15</sup> A. D. Caviglia, M. Gabay, S. Gariglio, N. Reyren, C. Cancellieri, and J.-M. Triscone, *Tunable Rashba Spin-Orbit Interaction at Oxide Interfaces*, Phys. Rev. Lett. 104 (2010), pp. 126803-1-126803-4. Available at <https://link.aps.org/doi/10.1103/PhysRevLett.104.126803>.
- <sup>16</sup> J. Lee, W. C. Tian, W. L. Wang and D. X. Yao, *Two-Dimensional Pnictogen Honeycomb Lattice: Structure, On-Site Spin-Orbit Coupling and Spin Polarization*, Sci. Rep. 5 (2015), pp. 11512-11528 . Available at <https://www.nature.com/articles/srep11512.pdf>.
- <sup>17</sup> F. Hellman, A. Hoffmann, Y. Tserkovnyak, G. S. D. Beach, E. E. Fullerton, C. Leighton, A. H. MacDonald, D. C. Ralph, D. Arena, H. A. Dürr, P. Fischer, J. Grollier, J. P. Heremans, T. Jungwirth, A. V. Kimel, B. Koopmans, I. N. Krivorotov, S. J. May, A. K. Petford-Long, J. M. and Rondinelli, N. Samarth, I. K. Schuller, A. N. Slavin, M. D. Stiles, O. Tchernyshyov, A. Thiaville, and B. L. Zink, *Interface-induced phenomena in magnetism*, Rev. Mod. Phys. 89 (2017), pp. 025006-1-025006-79. Available at <https://link.aps.org/doi/10.1103/RevModPhys.89.025006>.
- <sup>18</sup> A. Brinkman, M. Huijben, M. van Zalk, J. Huijben, U. Zeitler, J. C. Maan, W. G. van der Wiel, G. Rijnders, D. H. A. Blank, and H. Hilgenkamp, *Magnetic effects at the interface between non-magnetic oxides*, Nature Mater. 6 (2007), pp. 493-496. Available at <http://dx.doi.org/10.1038/nmat1931>.
- <sup>19</sup> S. Cao, M. Street, J. Wang, J. Wang, X. Zhang, C. Binek, P. Dowben, *Magnetization at the interface of Cr<sub>2</sub>O<sub>3</sub> and paramagnets with large stoner susceptibility*, J.Phys: Cond. Mat. 29 (2017), pp. 10LT01-1 - 10LT01-5 . Available at <http://iopscience.iop.org/article/10.1088/1361-648X/aa58ba/meta>
- <sup>20</sup> K. V. Raman and J. S. Moodera, *Materials chemistry: A magnetic facelift for non-magnetic metals*, Nature 524 (2015), pp. 42-43. Available at <https://www.nature.com/articles/524042a.pdf>.
- <sup>21</sup> T. Makarova, *Nanomagnetism in otherwise nonmagnetic materials*, Handbook of Nanophysics: Principles and Methods Vol. 1, CRC Press, Boca Raton, 2010. Available at arXiv, cond-mat/0207368.
- <sup>22</sup> E. Kovacs, R. Trencsenyi, Z. Gulacsi, *Magnetic nano-grains from a non-magnetic material: a possible explanation*, IOP Conf. Ser. 47 (2013), pp. 012048-1-012048-6. Available at <http://iopscience.iop.org/article/10.1088/1757-899X/47/1/012048/pdf>.
- <sup>23</sup> M. J. Pechan, E. E. Fullerton and I. K. Shuller, *Sources of interface magnetization and interface anisotropy in Fe/Cu multilayers as revealed by ther-*

- mal behavior*, Jour. Magn. Magn. Matter. 183 (1998), pp. 19-24. Available at <http://www.sciencedirect.com/science/article/pii/S0304885397010640KW>.
- <sup>24</sup> J. Huang, L. N. Pfeiffer and K. W. West, *Spin-orbit coupling and transport in strongly correlated two-dimensional systems*, Phys. Rev. B95 (2017), pp. 195139-1-195139-5. Available at <https://link.aps.org/doi/10.1103/PhysRevB.95.195139>.
- <sup>25</sup> S. Gangopadhyay and W. E. Pickett, *Interplay between spin-orbit coupling and strong correlation effects: Comparison of three osmate double perovskites: Ba<sub>2</sub>AOsO<sub>6</sub> (A=Na,Ca,Y)*, Phys. Rev. B93 (2016) pp. 155126-1 - 155126-10, Available at <https://journals.aps.org/prb/pdf/10.1103/PhysRevB.93.155126>
- <sup>26</sup> R. Schaffer, E. K. H. Lee, B. J. Yang and Y. B. Kim, *Recent progress on correlated electron systems with strong spin-orbit coupling*, Rep. Progr. Phys. 79 (2016), pp. 094504-1-094504-21 . Available at <http://iopscience.iop.org/article/10.1088/0034-4885/79/9/094504/pdf>.
- <sup>27</sup> L. Hao, D. Meyers, M. P. M. Dean and J. Liu, *Novel spin-orbit coupling driven emergent states in iridate-based heterostructures*, preprint (2017). Available at arXiv, cond-mat/1711.07609.
- <sup>28</sup> J. G. Rau, E. K. H. Lee and H. Y. Kee, *Spin-Orbit Physics Giving Rise to Novel Phases in Correlated Systems: Iridates and Related Materials*, Annual Review of Condensed Matter Physics 7 (2015), pp. 195-221. Available at <https://doi.org/10.1146/annurev-conmatphys-031115-011319>.
- <sup>29</sup> A. Farrell and T. P. Barnea, *Strong coupling expansion of the extended Hubbard model with spin-orbit coupling*, Phys. Rev. B89 (2014), pp. 035112-1-035112-16. Available at <https://link.aps.org/doi/10.1103/PhysRevB.89.035112>.
- <sup>30</sup> K. Hanzawa, K. Yosida and K. Yamada, *Susceptibility of the Periodic Anderson Model with Spin-Orbit Coupling*, Progr. Theor. Phys. 77 (1987), pp. 1116-1124. Available at <https://academic.oup.com/ptp/article/77/5/1116/1854685>.
- <sup>31</sup> A. A. Zvyagin, *Spin-orbit interaction in the supersymmetric antiferromagnetic  $tJ$  chain with a magnetic impurity*, Low Temp. Phys. 40 (2014), pp. 65-72. Available at <http://dspace.nbuv.gov.ua/bitstream/handle/123456789/119403/07-Zvyagin.pdf?sequence=1>.
- <sup>32</sup> H. Isobe and N. Nagaosa, *Enhancement of spin-orbit interaction by competition between Hund's coupling and electron hopping*, J. Phys: Conf. Ser. 592 (2015), pp. 012058-1-012058-6. Available at <http://iopscience.iop.org/article/10.1088/1742-6596/592/1/012058/pdf>.
- <sup>33</sup> A. Secchi, A. I. Lichtenstein and M. I. Katsnelson, *Magnetic interactions in strongly correlated systems: Spin and orbital contributions*, Annals of Phys. 360 (2015), pp. 61-97. Available at

<https://doi.org/10.1016/j.aop.2015.05.002>.

- <sup>34</sup> S. Chakraborty and A. Vijay, *Effective Hamiltonians for correlated narrow energy band systems and magnetic insulators: Role of spin-orbit interactions in metal-insulator transitions and magnetic phase transitions*, Jour. Chem. Phys. 144 (2016), pp. 144107-1-144107-14. Available at <http://aip.scitation.org/doi/full/10.1063/1.4945705>.
- <sup>35</sup> W. M. H. Natori, E. C. Andrade, E. Miranda and R. G. Pereira, *Chiral Spin-Orbital Liquids with Nodal Lines*, Phys. Rev. Lett. 117 (2016), pp. 017204-1 - 017204-5. Available at <https://link.aps.org/doi/10.1103/PhysRevLett.117.017204>.
- <sup>36</sup> L. Janssen, E. C. Andrade and M. Vojta, *Honeycomb-Lattice Heisenberg-Kitaev Model in a Magnetic Field: Spin Canting, Metamagnetism, and Vortex Crystals*, Phys. Rev. Lett. 117 (2016), pp. 277202-1-277202-5. Available at <https://link.aps.org/doi/10.1103/PhysRevLett.117.277202>.
- <sup>37</sup> Z. Gulácsi and D. Vollhardt, *Exact Insulating and Conducting Ground States of a Periodic Anderson Model in Three Dimensions*, Phys. Rev. Lett. 91 (2003), pp. 186401-1-186401-5. Available at <https://link.aps.org/doi/10.1103/PhysRevLett.91.186401>.
- <sup>38</sup> Z. Gulácsi, A. Kampf and D. Vollhardt, *Exact Many-Electron Ground States on the Diamond Hubbard Chain*, Phys. Rev. Lett. 99 (2007), pp. 026404-1-026404-4. Available at <https://link.aps.org/doi/10.1103/PhysRevLett.99.026404>.
- <sup>39</sup> Z. Gulácsi, A. Kampf and D. Vollhardt, *Route to ferromagnetism in organic polymers*, Phys. Rev. Lett. 105 (2010), pp. 266403-1-266403-4. Available at <https://link.aps.org/doi/10.1103/PhysRevLett.105.266403>.
- <sup>40</sup> Z. Gulácsi, *Exact ground states of correlated electrons on pentagon chains*, Int. Jour. Mod. Phys. B27 (2013), pp. 1330009-1-1330009-64. Available at <https://doi.org/10.1142/S0217979213300090>.
- <sup>41</sup> Z. Gulácsi, *Exact multi-electronic electron-concentration dependent ground-states for disordered two-dimensional two-band systems in presence of disordered hoppings and finite on-site random interactions.*, Phys. Rev. B69 (2004), pp. 054204-1-054204-10. Available at <https://link.aps.org/doi/10.1103/PhysRevB.69.054204>.
- <sup>42</sup> P. Gurin and Z. Gulácsi, *Exact solutions for the periodic Anderson model in two dimensions: A non-Fermi-liquid state in the normal phase*, Phys. Rev. B64 (2001), pp. 045118-1-045118-20. Available at <https://link.aps.org/doi/10.1103/PhysRevB.65.045118>.
- <sup>43</sup> Z. Gulácsi and D. Vollhardt, *Exact ground states of the periodic Anderson model*

- in  $D=3$  dimensions, Phys. Rev. B72 (2005), pp. 075130-1-075130-20. Available at <https://link.aps.org/doi/10.1103/PhysRevB.72.075130>.
- <sup>44</sup> Z. Gulácsi and M. Gulácsi, *Exact stripe, checkerboard, and droplet ground states in two dimensions*, Phys. Rev. B73 (2006), pp. 014524-1-014524-6. Available at <https://link.aps.org/doi/10.1103/PhysRevB.73.014524>.
- <sup>45</sup> Z. Gulácsi, *Delocalization effect of the Hubbard repulsion in exact terms and two dimensions*, Phys. Rev. B77 (2008), pp. 245113-1-245113-10. Available at <https://link.aps.org/doi/10.1103/PhysRevB.77.245113>.
- <sup>46</sup> R. Trencsényi, E. Kovács and Z. Gulácsi, *Correlation and confinement induced itinerant ferromagnetism in chain structures*, Phil. Mag. 89 (2009), pp. 1953-1974. Available at <https://doi.org/10.1080/14786430902810498>.
- <sup>47</sup> R. Trencsényi and Z. Gulácsi, *The emergence domain of an exact ground state in a non-integrable system: the case of the polyphenylene type of chains*, Phil. Mag. 92 (2012), pp. 4657-4675. Available at <http://www.tandfonline.com/doi/full/10.1080/14786435.2012.716527>
- <sup>48</sup> Gy. Kovács, Z. Gulácsi, *Pentagon chain in external fields*, Phil. Mag. 95 (2015), pp. 3674-3695. Available at <http://www.tandfonline.com/doi/abs/10.1080/14786435.2015.1094191>.
- <sup>49</sup> Z. Yu, *Short-range correlations in dilute atomic Fermi gases with spin-orbit coupling*, Phys. Rev. A85 (2012), pp. 042711-1-042711-7. Available at <https://link.aps.org/doi/10.1103/PhysRevA.85.042711>.
- <sup>50</sup> P. Boross, B. Dora, A. Kiss, and F. Simon, *A unified theory of spin-relaxation due to spin-orbit coupling in metals and semiconductors*, Sci. Rep. 3 (2013), pp. 3233-3238. Available at <https://www.nature.com/articles/srep03233.pdf>.
- <sup>51</sup> Z. Li, L. Covaci and F. Marsiglio, *Impact of Dresselhaus vs. Rashba spin-orbit coupling on the Holstein polaron*, Phys. Rev. B85 (2012), pp. 205112-1-205112-5. Available at <https://link.aps.org/doi/10.1103/PhysRevB.85.205112>.
- <sup>52</sup> M. Kollar, D. Strack and D. Vollhardt, *Ferromagnetism in Correlated Electron Systems: Generalization of Nagaoka's Theorem*, Phys. Rev. B53 (1996), pp. 9225-9231. Available at <https://link.aps.org/doi/10.1103/PhysRevB.53.9225>.
- <sup>53</sup> O. O. Brovko, P. Ruiz-Diaz, T. R. Dasa and V. S. Stepanyuk, *Controlling magnetism on metal surfaces with non-magnetic means: electric fields and surface charging*, Jour. Phys: Cond. Matter 26 (2014), pp. 093001-1-093001-25. Available at

<http://stacks.iop.org/0953-8984/26/i=9/a=093001>.

- <sup>54</sup> One notes that since for  $\lambda_f = 0$  the ground state (8) is no more valid, the plot in Fig.4 cannot be started from the origin. But the relation  $\lim_{\lambda_f \rightarrow 0} \bar{S}_n^z = 0$  is satisfied.
- <sup>55</sup> T. Hotta, *Existence of a novel metallic ferromagnetic phase in models for undoped manganites*, Phys. Rev. B67 (2003), pp. 104428-1-104428-8. Available at <https://link.aps.org/doi/10.1103/PhysRevB.67.104428>.
- <sup>56</sup> Z. Gulácsi, R. Strack and D. Vollhardt, *Accurate variational results for the symmetric periodic Anderson model in one, two, and three dimensions*, Phys. Rev. B47 (1993), pp. 8594-8604. Available at <https://link.aps.org/doi/10.1103/PhysRevB.47.8594>.
- <sup>57</sup> B. Möller and P. Wölfle, *Magnetic order in the periodic Anderson model*, Phys. Rev. B48 (1993), pp. 10320-10326. Available at <https://link.aps.org/doi/10.1103/PhysRevB.48.10320>.
- <sup>58</sup> J. Goraus, *Onsite hybridization between Ce 4f and 5d states as the indicator of the transition from Kondo insulator to metallic state in CeRhSb*, Phys. Lett. A375 (2011), pp. 3469-1-3469-4. Available at <https://www.sciencedirect.com/science/article/pii/S0375960111009479>.